Table 1. Experimental and calculated values for $AuXe_4^{2+}$.

	Experimental	HF*	Becke3LYP†	MP‡
Au-Xe bond length (pm)	272.8(1)–275.0(1)	289.1	287.1	278.7
Mulliken charges				
Au	–	+0.50	+0.13	+0.34
Xe	–	+0.37	+0.47	+0.41
ΔH (kcal mol^{-1})				
$Au^{2+} + 4Xe \rightarrow AuXe_4^{2+}$	–	−144	−228	−199

*Hartree-Fock ab initio calculation with a core potential for the inner 60 electrons and a 6s5p3d basis set for Au, and a 4s4p3d1f basis set and a core potential for the inner 46 electrons for Xe (*10*). †Density functional calculation with the Becke3 method (*14*) and the correction by Lee, Yang, and Parr (*15*); same basis set as in the Hartree-Fock calculation. ‡Møller-Plesset second-order calculation; same basis set as in the Hartree-Fock calculation.

gold may not be different from that between xenon and any electronegative main-group element, such as in XeF_2. Here, a charge transfer of about 0.5 electrons to the electronegative fluorine atom is assumed (*12*).

During the reduction of Au^{3+} to Au^{2+} and the complexation of Au^{2+}, the extreme Brønsted acidity of the HF/SbF_5 solution is essential. The Au^{3+} ion in fluoride systems is normally present as AuF_4^-, which when protonated, can ultimately lead to $Au(HF)_4^{3+}$, which has a much higher oxidation potential than AuF_4^-. It can almost be considered as a naked Au^{3+} ion due to the weak basicity of HF. The complexation reaction must be an equilibrium $Au^{2+}(HF)_n + 4Xe \leftrightarrows AuXe_4^{2+} + nHF$, which again can only proceed if xenon remains the strongest base in the system. The overall reaction indicates yet again the role of the protons

$$AuF_3 + 6Xe + 3H^+ \rightarrow AuXe_4^{2+} + Xe_2^+ + 3HF$$

Green $Xe_2^+Sb_4F_{21}^-$ crystals, which have been fully characterized previously (*13*), were also detected in the solid reaction mixture at −60°C.

The isolation of the $AuXe_4^{2+}$ cation raises many questions that at present cannot be answered satisfactorily. The main question is, of course, whether this compound remains unique or if this is the first of a series of new complexes. Predictions are difficult because this first compound is also unique in another way: Stoichiometry and structure for a Au^{2+} complex are rare if not entirely new.

References and Notes

1. N. Bartlett, *Proc. R. Chem. Soc.* **1962**, 218 (1962).
2. M. B. Simpson, M. Poliakoff, J. J. Turner, W. B. Maier II, J. G. McLaughlin, *J. Chem. Soc. Chem. Commun.* **1983**, 1355 (1983); B. H. Weiller, *J. Am. Chem. Soc.* **114**, 10911 (1992); S. A. Fairhurst, J. R. Morton, R. N. Perutz, K. F. Preston, *Organometallics* **3**, 1389 (1984); J. R. Wells and E. Weitz, *J. Am. Chem. Soc.* **114**, 2783 (1992); A. W. Ehlers, G. Frenking, E. J. Baerends, *Organometallics* **16**, 4896 (1997).
3. X.-Z. Sun, D. C. Grills, S. M. Nikiforov, M. Poliakoff, M. W. George, *J. Am. Chem. Soc.* **119**, 7521 (1997); B. H. Weiller, E. P. Wasserman, R. J. Bergman, C. B. Moore, G. C. Pimentel, *J. Am. Chem. Soc.* **111**, 8288 (1989); B. H. Weiller, E. P. Wasserman, C. B. Moore, R. B. Bergman, *J. Am. Chem. Soc.* **115**, 4326 (1993); R. H. Schultz *et al.*, *J. Am. Chem. Soc.* **116**, 7369 (1994); A. A. Bengali, R. H. Schultz, C. B. Moore, R. G. Bergman, *J. Am. Chem. Soc.* **116**, 9585 (1994); A. A. Bengali, R. G. Bergman, C. B. Moore, *J. Am. Chem. Soc.* **117**, 3879 (1995); B. K. McNamara, J. S. Yeston, R. G. Bergman, C. B. Moore, *J. Am. Chem. Soc.* **121**, 6437 (1999).
4. D. Schröder, H. Schwarz, J. Hrušák, P. Pyykkö, *Inorg. Chem.* **37**, 624 (1998). For a previous calculation on $AuXe^+$ and $AuXe_2^+$, see also P. Pyykkö, *J. Am. Chem. Soc.* **117**, 2067 (1995).
5. C. J. Evans, A. Lesarri, M. C. L. Gerry, *J. Am. Chem. Soc.* **122**, 6100 (2000).
6. L. Graham, O. Graudejus, N. K. Jha, N. Bartlett, *Coord. Chem. Rev.* **197**, 321 (2000).
7. R. Küster and K. Seppelt, *Z. Anorg. Allg. Chem.* **626**, 236 (2000).
8. S. H. Elder, G. M. Lucier, F. J. Hollander, N. Bartlett, *J. Am. Chem. Soc.* **119**, 1020 (1997).
9. $AuXe_4^{2+}(Sb_2F_{11}^-)_2$ crystal parameters: Cell dimensions a = 794.0 ± 1 pm, b = 917.7 ± 1 pm, c = 1739.1(3) pm, α = 99.539 ± 5°, β = 92.640 ± 4°, γ = 94.646 ± 5°, unit cell volume $V = 1243.4 \times 10^6$ pm^3, temperature T = −120°C; space group $P\bar{1}$, number of molecular units in the unit cell Z = 2, calculated density ρ_{calc} = 3.696 g/cm^3, absorption correction by equalizing symmetry-related reflections with absorption coefficient μ = 13.55 mm^{-1}. MoKα rays with graphite monochromator, 33,456 measured reflections, 8837 unique reflections, max diffraction angle θ_{max} = 31°, 281 refined parameters, all atoms were refined anisotropically, full least-square matrix refinement, reliability factor $R[F \geq 4\sigma(F)] = 0.039$, weighed reliability factor based on R^2 $wR_2 = 0.099$, weighing scheme $w = 1/\sigma^2[F(o)^2 + (0.0576P)^2 + 1.98P$, $P = \max[F(o)^2,0]^+ \ 2Fc^2/3$. Further details on the crystal structure determination can be obtained from the Fachinformationszentrum Karlsruhe, 76344 Eggenstein-Leopoldshafen, Germany [Fax: (+49)7247-808-6666; E-mail: crysdata@fiz-karlsruhe.de, accession number CSD 411365].
10. Calculations were done with the program Gaussian 98, Revision E.2 [M. J. Risch *et al.*, Gaussian, Inc., Pittsburgh, PA, 1995]. Basis sets and core potentials were obtained from the Institut für Theoretische Chemie, Universität Stuttgart, Germany.
11. P. Pyykkö and J. P. Desclaux, *Acc. Chem. Res.* **12**, 276 (1979).
12. N. Bartlett and F. O. Sladky, in *Comprehensive Inorganic Chemistry*, J. C. Bailar and H. J. Emeleus, Eds. (Pergamon, Oxford, 1973), vol. 1, p. 226.
13. T. Drews and K. Seppelt, *Angew. Chem. Int. Ed. Engl.* **36**, 273 (1997).
14. A. D. Becke, *J. Chem. Phys.* **98**, 5648 (1993).
15. C. Lee, W. Yang, R. G. Parr, *Phys. Rev. B* **37**, 785 (1988).

30 June 2000; accepted 31 August 2000

Resurrection of Crushed Magnetization and Chaotic Dynamics in Solution NMR Spectroscopy

Yung-Ya Lin, Natalia Lisitza, Sangdoo Ahn, Warren S. Warren*

We show experimentally and theoretically that two readily observed effects in solution nuclear magnetic resonance (NMR)—radiation damping and the dipolar field—combine to generate bizarre spin dynamics (including chaotic evolution) even with extraordinarily simple sequences. For example, seemingly insignificant residual magnetization after a crusher gradient triggers exponential regrowth of the magnetization, followed by aperiodic turbulent spin motion. The estimated Lyapunov exponent suggests the onset of spatial-temporal chaos and the existence of chaotic attractors. This effect leads to highly irreproducible experimental decays that amplify minor nonuniformities such as temperature gradients. Imaging applications and consequences for other NMR studies are discussed.

Modern high-resolution liquid-state nuclear magnetic resonance (NMR) and magnetic resonance imaging (MRI) experiments often include a complex sequence of radio frequency (RF) pulses for creating and transferring spin coherence and pulsed-field gradients for coherence pathway selection, rejection, and spatial encoding. The full spin evolution under such sequences is readily calculated even for molecules as large as proteins within the density matrix framework, and such calculations have proven invaluable for pulse sequence optimization and extraction of molecular parameters. Recent work on dipolar field effects in water and other solvents has explained previously

---

Department of Chemistry, Princeton University, Princeton, NJ 08544, USA.

*To whom correspondence should be addressed. E-mail: wwarren@princeton.edu

unexpected spectral features (such as detection of intermolecular multiple-quantum coherences) (*1–3*) and has predicted some new applications (*4–6*) but has not challenged the essentially predictable and reproducible nature of this approach. In contrast, this paper presents experimental and numerical evidence that two readily observed effects in concentrated solutions—radiation damping and the dipolar field—combine to generate chaotic dynamics even with extraordinarily simple sequences.

Consider the simplest pulse/gradient combination $[(\pi/2)_x - (GT)_z]$: an RF pulse along the x axis with a flip angle of $\pi/2$ followed by a "crusher" B_0 gradient in the z direction with strength G and duration time T. Such a scheme appears in a wide range of experiments, including imaging and solvent suppression. The $\pi/2$ pulse tips the magnetization into the transverse plane. The crusher gradient then spatially modulates the transverse magnetization, creating a magnetization grating. The modulated magnetization is expected to give no signal in the absence of additional refocusing gradients; only a tiny residual magnetization, about 10^{-3} to 10^{-5} of the equilibrium magnetization, typically survives the crusher gradient (arising, for example, from a noninteger number of helix cycles, static-field inhomogeneity, and spectrometer imperfections) (*7*).

Instead, for a concentrated sample the "crushed" magnetization revives over the course of many milliseconds; the residual magnetization is amplified (typically by a factor of 100 to 10,000) before it decays away (Fig. 1). This effect is very well known in the biological NMR community; the difficulty of suppressing the water peak and having it stay suppressed has relegated many promising two-dimensional NMR sequences to experimental oblivion (*7*). Most modern experiments are constrained to use "water flip-back" pulses to restore the magnetization to the z axis, even if this procedure compromises other aspects of the pulse sequence design (*8*).

The explanation for this unexpected reappearance turns out to be rather subtle. The fundamental physics can be described by modified (nonlinear) Bloch equations. We define the dimensionless normalized Bloch vector $\boldsymbol{m}(\boldsymbol{r}) \equiv \boldsymbol{M}(\boldsymbol{r})/M_0$, where $\boldsymbol{M}(\boldsymbol{r})$ is the magnetization density vector of a small volume element at position $\boldsymbol{r}$ in the sample and M_0 is the equilibrium magnetization under the external Zeeman field of flux density B_0 along the z axis. For equivalent spins in a liquid (such as water or acetone), the effective spin dynamics in the rotating frame precessing with the Larmor frequency $\omega_0 = \gamma B_0$ can be approximated as (*9*)

$$\frac{\partial \boldsymbol{m}}{\partial t} = \gamma \boldsymbol{m} \times \boldsymbol{B} - \frac{m_x\hat{\boldsymbol{x}} + m_y\hat{\boldsymbol{y}}}{T_2} - \frac{m_z - 1}{T_1}\hat{\boldsymbol{z}} + \mathrm{D}\nabla^2\boldsymbol{m} \qquad (1)$$

where γ is the gyromagnetic ratio, $\boldsymbol{B}(\boldsymbol{r}, t)$ is the local field acting on $\boldsymbol{m}(\boldsymbol{r}, t)$, T_1 and T_2 are, respectively, the longitudinal and transverse relaxation times, D is the diffusion coefficient, and $\{\hat{\boldsymbol{x}}, \hat{\boldsymbol{y}}, \hat{\boldsymbol{z}}\}$ are the basis vectors of the Cartesian coordinates. The macroscopic experimental observable $\langle \boldsymbol{m} \rangle$ is obtained by averaging $\boldsymbol{m}$ over all of the volume elements in the sample.

The initial condition after the preparation of $[(\pi/2)_x - (GT)_z]$ can be written almost exactly as

$$m_+(z,0) = \exp(i\gamma GTz), \quad m_x(z,0) = 0 \qquad (2)$$

where $m_+ = m_x + im_y$; as noted above, for a realistic gradient, there will be some small deviations that lead to a small but nonzero value of $\langle m_+ \rangle$.

In the usual (linear) version of Eq. 1, the local field $\boldsymbol{B}(\boldsymbol{r}, t)$ is independent of $\boldsymbol{m}(\boldsymbol{r}, t)$, and macroscopic transverse magnetization $\langle m_+ \rangle$ should never reappear. For concentrated samples of abundant high-γ spins in a high-resolution NMR spectrometer, additional contributions to the local field come from radiation damping $\boldsymbol{B}_r$ (*9*, *10*) and the distant dipole field (DDF) $\boldsymbol{B}_d$, that is, $\boldsymbol{B} = \boldsymbol{B}_d + \boldsymbol{B}_r$ (*11*, *12*). Radiation damping is a macroscopic reaction field, which is fed back to the spins through the induced free-induction-decay (FID) current in the receiver coil. As dictated by Lenz's law, it exerts a torque to nutate $\boldsymbol{m}$ all the way back to the $+z$ axis on the surface of the Bloch sphere and, when the sample is exactly on resonance, can be described by

$$\gamma \boldsymbol{B}_r = \frac{1}{\tau_r}\left(- \langle m_y \rangle \hat{\boldsymbol{x}} + \langle m_x \rangle \hat{\boldsymbol{y}} \right),$$

$$\tau_r = \frac{1}{2\pi\gamma\eta M_0 Q} \qquad (3)$$

where η is the filling factor of the coil and Q is the probe Q factor. However, this correction would be expected to have little effect after a $[(\pi/2)_x - (GT)_z]$ sequence, because most of the transverse magnetization has been suppressed.

Finally, the DDF arises from residual dipolar couplings in solution. The coupling can be handled in two superficially different ways, which give the same results (*3*, *13*). First, retain the dipolar couplings explicitly, and model them as affecting the time evolution through commutation (*1*, *3*). In this "quantum" or "coupled-spin" picture, everything remains in operator form, virtually identical to the normal treatment for a solid. The other alternative is to make the mean field approximation. This "classical" or "mean-field" treatment introduces the DDF, which can be treated as a microscopic reaction field. It was first introduced to explain multiple echoes in a continuous gradient (*11*). In the cases where the magnetization is fully modulated and varies only in one direction s, it can be approximated as (*12*)

$$\gamma \boldsymbol{B}_d = \frac{1}{\tau_d}\Delta_s \times \left\{ [m_z(s) - \langle m_z \rangle]\hat{\boldsymbol{z}} - \frac{1}{3}[\boldsymbol{m}(s) - \langle \boldsymbol{m} \rangle] \right\} \qquad (4)$$

where $\Delta_s = [3(\boldsymbol{s} \cdot \boldsymbol{z})^2 - 1]/2$, $\tau_d = (\gamma\mu_0 M_0)^{-1}$, and μ_0 is the magnetic permeability of a vacuum. For z gradient–modulated magnetization, $\Delta_s = 1$, but after a $[(\pi/2)_x - (GT)_z]$ sequence, $m_z \approx 0$ everywhere, and $\langle \boldsymbol{m} \rangle$ is small, so the dipolar field is nearly linearly proportional to $\boldsymbol{m}$; thus the cross product in Eq. 1 eliminates any effects on the spin evolution.

The results of this trivially simple experiment disagree with these expectations. In the limit where either radiation damping or DDF dominates, a solid theoretical framework exists to describe the corresponding dynamics (at least if spatial inhomogeneities can be ignored), and many gradient experiments with dipolar fields have been successfully described by ignoring radiation damping. However, the comparable characteristic times, $\tau_r \approx 10$ ms and $\tau_d \approx 65$ ms for a pure water sample in a typical 600-MHz spectrometer at room temperature, imply that it might be crucial to take their joint action into account for some experiments. It turns out that the simple one-pulse, one-gradient sequence fits into

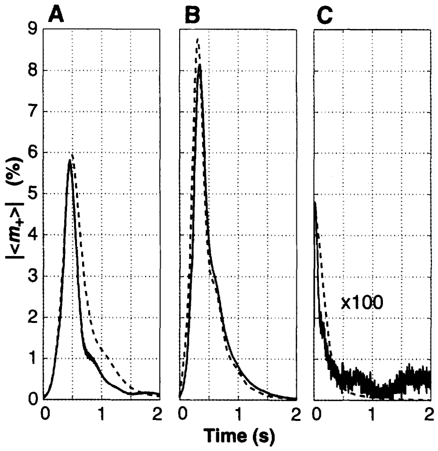

Fig. 1. Experimental (solid lines) and simulated (dotted line) ^{1}H FIDs (absolute magnitude) of 95% water on a D_2O-locked Varian INOVA 600 MHz spectrometer after the sequence $[(\pi/2)_x - (GT)_z]$. The sample temperature was stabilized at 25°C for 2 hours before data acquisition. **(A)** A z gradient with optimal shimming. **(B)** A z gradient with ~1.5 Hz/cm linear B_0 inhomogeneity. **(C)** A magic-angle gradient with optimal shimming (note scale change), which confirms that DDF is a prerequisite for the resurrection process. The following parameters are estimated from experiments and then used in the simulations: acquisition delay 50 s, $GT = 2.5$ gauss · ms/cm, $T_1 = 3.05$ s, $T_2 = 2.10$ s, $\tau_r = 10$ ms, $\tau_d = 69.8$ ms, $D = 1.85 \times 10^{-5}$ cm^2/s, and residual line-broadening = 0.4 Hz. The details of the numerical simulations are described in reference (*15*).

this category, and simulation results shown in Figs. 1 to 3 explain the observed recurrence well (for samples without temperature gradients). To gain insight, we can generate approximate solutions by temporarily ignoring the T_1, T_2, and diffusion processes in Eq. 1. Addition of another pulse of flip angle θ after the gradient would have converted intermolecular zero-quantum coherences (iZQC) into two-spin, single-quantum coherences, which become observable by the action of the DDF (*3*, *5*, *6*). In such a "ZQ CRAZED" or HOMOGENIZED sequence, the signal at a time t after the second pulse would be given by

$$\langle m_+\rangle = -i\cos\theta J_1(t\sin\theta/\tau_d) \qquad (5)$$

where J_1 is the first-order Bessel function. Such sequences usually use a second pulse flip angle of $\theta = \pi/4$ to maximize the initial magnetization growth. However, note that as θ approaches zero, the maximum possible signal (ignoring relaxation) actually grows, in principle, to almost the full equilibrium magnetization, although it appears at a later time as θ decreases.

The effect of radiation damping, starting even with a very small residual magnetization ε, is to create a second pulse with a very small flip angle. This second pulse triggers magnetization growth in Eq. 5, which in turn creates an even larger pulse through radiation damping; further amplifies the transverse magnetization, and begins to create z-magnetization as well. Numerical simulations without relaxation and diffusion (shown in Fig. 2) show that under ideal experimental conditions the magnetization can reach ~17% and ~46% of the equilibrium magnetization for $|\langle m_+\rangle|$ and $\langle m_z\rangle$, respectively.

This powerful positive feedback occurs on a time scale $\sqrt{\tau_r\tau_d}$ that is much shorter than relaxation times in solution, and thus instabilities in the dynamics are not surprising. The aperiodic turbulent spin motion shown in Fig. 2 suggests the onset of spatial-temporal chaos and the existence of chaotic attractors. The system is sensitive to initial conditions, and neighboring trajectories separate exponentially fast. This divergence is plotted in Fig. 3 as the spread of the Bloch vectors $\boldsymbol{m}(\boldsymbol{r},t)$ at various times for 500 slightly perturbed initial conditions. Around one of the attractors (at 1.5 s), all neighboring trajectories converge, which gives rise to one of the gradient echoes in the FID. The largest Lyapunov exponent for the whole system is approximately 0.96 s^{-1}, following the algorithm of (*14*). The chaotic character disappears if either radiation damping or the DDF is removed from these simulations, which assume the magnetization fluctuates in only one dimension (thus making Eq. 4 valid). Evolution with small three-dimensional fluctuations [using the simulation method of (*15*)] also appears to show chaotic dynamics, even without radiation damping, but on a longer time scale. This is consistent with the results of (*16*), which predicted that dynamical effects of the dipolar field inhomogeneities would induce spectral clustering and instabilities.

In real experiments, the underlying dynamics leads to signal instability, amplifying deviations from a uniformly modulated magnetization. For example, any residual B_0 inhomogeneity behaves mostly as a weak z gradient (for samples that are longer than they are wide) to perturb the helix structure. This effect usually can be safely ignored, as the irreversible relaxations will smear the helix structure before the small B_0 inhomogeneity can exhibit any significant effect. However, here a small B_0 inhomogeneity can work in concert with the nonlinear dynamics to accelerate the resurrection process and to drive $|\langle m_+\rangle|$ to a higher maximum value (Figs.1 and 4). The results of magic-angle gradient experiments ($\Delta_s = 0$ in Eq. 4), shown in Fig. 1C, confirm that DDF is indeed a prerequisite for the resurrection. As the B_0 inhomogeneity continues to increase, it eventually dominates the helix modulation mechanism and makes other effects invisible. The exponential growth is counterbalanced by relaxation; for spin systems subject to less significant relaxation effects, larger recurrences are possible.

A more dramatic example is shown in Fig. 5. Figure 5A shows 128 superimposed transients from the $[(\pi/2)_x - (GT)_z]$ sequence in a 600-MHz NMR spectrometer, with the sample temperature stabilized at 25°C for 2 hours before data acquisition

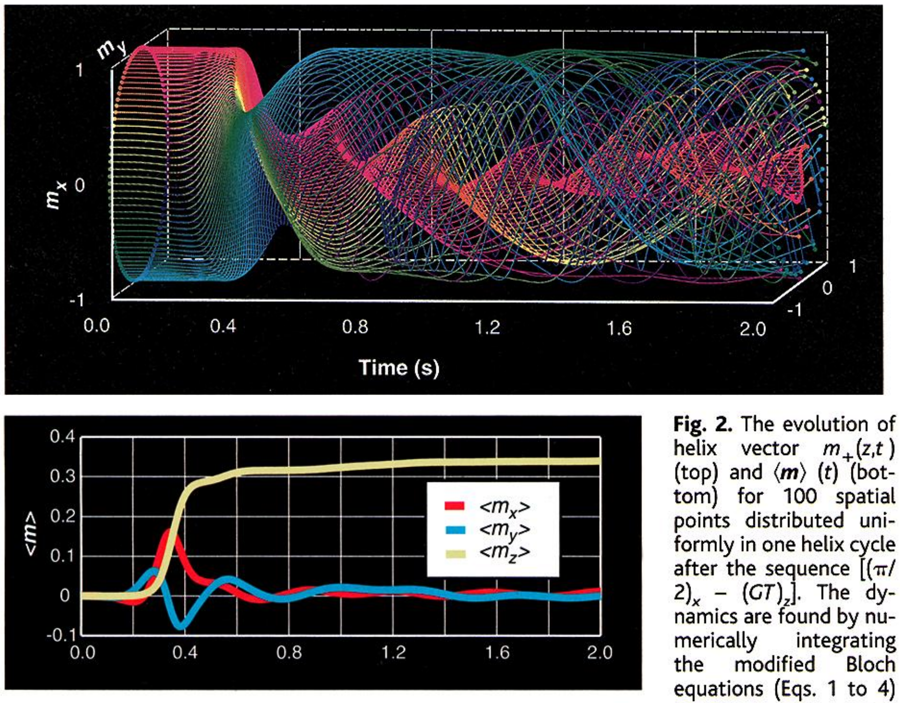

Fig. 2. The evolution of helix vector $m_+(z,t)$ (top) and $\langle \boldsymbol{m}\rangle(t)$ (bottom) for 100 spatial points distributed uniformly in one helix cycle after the sequence $[(\pi/2)_x - (GT)_z]$. The dynamics are found by numerically integrating the modified Bloch equations (Eqs. 1 to 4) based on the finite element method and Runge-Kutta (4,5) algorithm without T_1, T_2, and diffusion effects. The different initial $m_+(z,t)$ values along one helical turn are mapped onto a plane; the long-time evolution shows the trajectory divergence. The physical parameters used are: τ_r = 10 ms, τ_d = 69.8 ms, GT = 5 gauss · ms/cm, $\varepsilon = 1.0 \times 10^{-3}$, and L = 0.9395 cm (sampled by 2000 spatial points along z axis). This simulation assumes magnetization fluctuations in one dimension (see text).

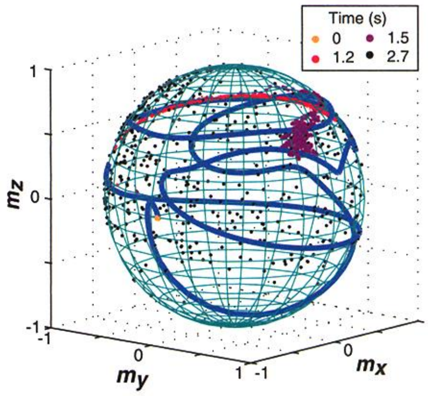

Fig. 3. The exponentially fast divergence of 500 neighboring trajectories of the microscopic magnetization vector at the specific position $\boldsymbol{m}(z,0) = [-1,0,0]$ after the sequence $[(\pi/2)_x - (GT)_z]$ for the system shown in Fig. 2. The spread in the initial conditions at that specific position is created by uniformly distributed random numbers within the range of ±0.01 in m_x, m_y, and m_z, respectively, while keeping the initial conditions at all other positions fixed.

(the room temperature stayed between 22° and 23°C). The fluctuations are small, but still larger than expected; the maximum of the fluctuations in the magnitude of the normal FIDs acquired with a single $\pi/2$ pulse under similar experimental conditions discussed here is only about 3×10^{-4} (standard deviation), which would not be observable at all on this scale. If we raise the temperature to 30°C and wait 2 hours for the system to stabilize, fluctuations in the normal FID are still virtually unobservable, but fluctuations in the $[(\pi/2)_x - (GT)_z]$ sequence are large (Fig. 5B); the stronger temperature gradients create a spatially modulated DDF. Superimposed transients beginning 30 min after a magnet fill are shown in Fig. 5C. Again the normal FID amplitude is very stable (the heater keeps the average sample temperature fixed), but the $[(\pi/2)_x - (GT)_z]$ sequence signal fluctuates wildly. The very small temperature gradients imply magnetization nonuniformity and instability, which generates perturbations in the DDF. The shapes of the individual FIDs change dramatically as well, implying that this effect is not simply amplification of some nonreproducible, initial unsuppressed magnetization, although that may contribute to the initial growth.

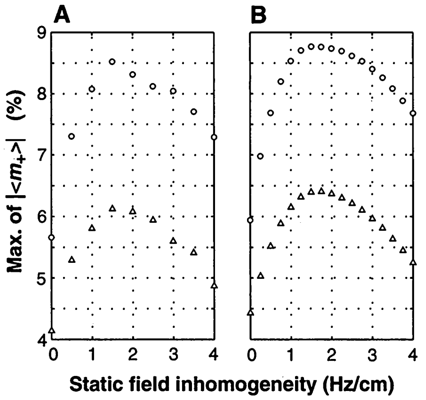

Fig. 4. Maximum value of absolute magnitude reached during the resurrection of the macroscopic transverse magnetization with various static-field inhomogeneity after the sequence $[(\pi/2)_x - (GT)_z]$. (**A**) Experimental average of 128 scans. (**B**) Simulations for 95% water with GT = 2.5 gauss · ms/cm (triangles) or 5 gauss · ms/cm (circles). The other parameters are the same as those listed in Fig. 1.

The ultimate limit to magnetization uniformity is dictated by the finite number of spins per unit volume, that is, the spin noise. For example, suppose the magnetization is modulated by a gradient pulse of strength 8 G/cm and duration 1 ms (typical for many of our experiments). The magnetization helix then has a repeat distance of 300 μm, or a "correlation distance" of 150 μm. The volume in a slice this thick (1 μL) contains 7×10^{19} spins. In a canonical ensemble, the ratio of the spontaneous fluctuations $[(7 \times 10^{19})^{-1/2}]$ to the equilibrium magnetization $[\approx(5 \times 10^{-5})$ of the zero-temperature magnetization] is on the of order 10^{-6}. Our simulations show that this much variation, when coupled with sufficiently large initial residual magnetization ε (for example, 1%), is sufficient to generate unpredictable and irreproducible trajectories at long times. As will be shown elsewhere, this unexpected mechanism can severely deteriorate pulse sequence performance. For example, the recovering magnetization would also contribute to "t_1 noise" in a variety of multidimensional NMR experiments, where solvent is suppressed by gradient pulses, and this instability may well be the origin of the poor performance of gradient-based solvent suppression in NMR. Fortunately, in many cases such effects can be minimized by either magic-angle gradients, as shown here, or by active feedback to suppress radiation damping (*17*).

The dipolar field has already been shown to provide a fundamentally new contrast mechanism in MRI that is sensitive to magnetization variations over subvoxel distances (*6*). Figure 5 suggests that the unstable dynamics and amplification of small magnetization variations might be usable in imaging or detecting these variations and might provide another tool for investigation of microscopic structure. In recent years, magnetic chaos or magnetic turbulence has been demonstrated in parametric pumping, spin chains, and NMR masers (*18*, *19*). Our work presented here reveals the existence of instability and apparently chaotic dynamics under routinely accessible conditions for solution NMR spectroscopy. This appears on a faster time scale than would be predicted by the approach in (*16*): nonlinearity triggered by the joint action of radiation damping and the DDF amplifies the effects of nonuniformity, and creates a macroscopic signal. With the trend of designing supersensitive probes and high-field magnets for biological systems with concentrated high-γ solvents, one can expect that this nonlinear effect will become even more pronounced. In this regard, understanding of the underlying chaotic dynamics and the control of the resurrection process may be critical to further developments and applications of high-resolution NMR in liquids.

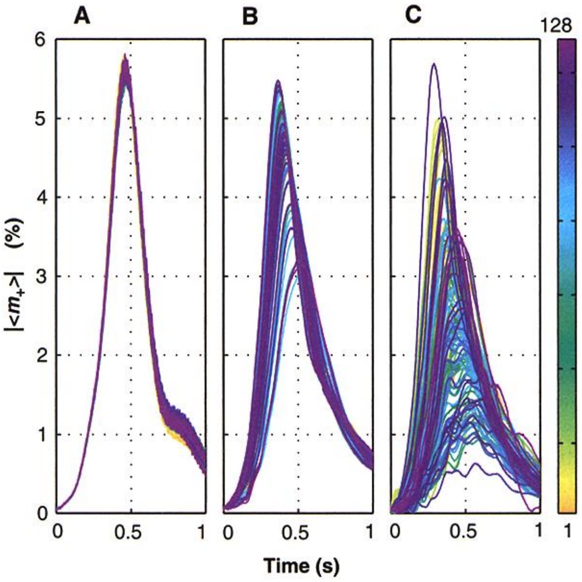

Fig. 5. Superimposition of 128 experimental ^{1}H FIDs (absolute magnitude) of 95% water after the sequence $[(\pi/2)_x - (GT)_z]$, with the sample temperature stabilized (**A**) at 25°C for 2 hours before data acquisition, (**B**) at 30°C for 2 hours before data acquisition, and (**C**) at 25°C beginning 30 min after a magnet fill. The other experimental conditions are the same as those in Fig. 1. The maximum of the fluctuations in the magnitude of the normal FIDs acquired with a single $\pi/2$ pulse under similar experimental conditions discussed here is only about 3×10^{-4} (standard deviation), which would not be observable at all on this scale.

References and Notes

1. W. S. Warren, W. Richter, A. H. Andreotti, B. T. Farmer II, *Science* **262**, 2005 (1993).
2. Q. He, W. Richter, S. Vathyam, W. S. Warren, *J. Chem. Phys.* **98**, 6779 (1993).
3. S. Lee, W. Richter, S. Vathyam, W. S. Warren, *J. Chem. Phys.* **105**, 874 (1996).
4. W. Richter, S. Lee, W. S. Warren, Q. He, *Science* **267**, 654 (1995).
5. S. Vathyam, S. Lee, W. S. Warren, *Science* **272**, 92 (1996).
6. W. S. Warren *et al.*, *Science* **281**, 247 (1998).
7. M. Gueron, P. Plateau, M. Decorps, *Prog. NMR Spectrosc.* **23**, 135 (1991).
8. A. Bax, V. Sklenar, G. M. Clore, A. M. Gronenborn, *J. Am. Chem. Soc.* **109**, 6511 (1987).
9. A. Abragam, *Principles of Nuclear Magnetism* (Clarendon, Oxford, 1961).
10. N. Bloembergen and R. V. Pound, *Phys. Rev.* **95**, 8 (1954).
11. G. Deville, M. Bernier, J. M. Delrieux, *Phys. Rev. B* **19**, 5666 (1979); H. T. Edzes, *J. Magn. Reson.* **86**, 293 (1990); R. Bowtell, R. M. Bowley, P. Glover, *J. Magn. Res.* **88**, 643 (1990).
12. W. S. Warren, S. Lee, W. Richter, S. Vathyam, *Chem. Phys. Lett.* **247**, 207 (1995).
13. J. Jeener, *J. Chem. Phys.* **112**, 5091 (2000); J. Jeener, A. Vlassenbroek, P. Broekaert, *J. Chem. Phys.* **103**, 1309 (1995).
14. T. S. Parker and L. O. Chua, *Practical Numerical Algorithms for Chaotic Systems* (Springer-Verlag, New York, 1989).
15. T. Enss, S. Ahn, W. S. Warren, *Chem. Phys. Lett.* **305**, 101 (1999); S. Garrett-Roe and W. S. Warren, *J. Magn. Reson.* **146**, 1 (2000).
16. J. Jeener, *Phys. Rev. Lett.* **82**, 1772 (1999).
17. P. Broekaert and J. Jeener, *J. Magn. Reson. A* **113**, 60 (1995).
18. R. Badii *et al.*, *Rev. Mod. Phys.* **66**, 1389 (1994).
19. K. N. Alekseev, G. P. Berman, V. I. Tsifrinovich, A. M. Frishman, *Sov. Phys. Usp.* **35**, 572 (1992).
20. This work was supported by the NIH under grant GM35253.

21 June 2000; accepted 21 August 2000